Electrodeposition of High-Purity Indium Thin Films and Its Application to Indium Phosphide Solar Cells

Peter Lobaccaro,[a,b] Anahit Raygani,[a,c,*] Andrea Oriani,[a,c,*] Nicolas Miani,[a,c] Alessandro Piotto,[a,c] Rehan Kapadia,[b,d,] Maxwell Zheng,[b,d] Zhibin Yu,[b,d] Luca Magagnin,[c,**] Daryl C. Chrzan,[b,e] Roya Maboudian,[a,**,z] and Ali Javey[b,d,z]**

[a]*Chemical and Biomolecular Engineering, University of California, Berkeley, California 94704, USA*
[b]*Materials Sciences Division, Lawrence Berkeley National Laboratory, Berkeley, California 94720, USA*
[c]*Dip. Chimica, Materiali e Ing. Chimica, G. Natta Politecnico di Milano, Milano 20133, Italy*
[d]*Electrical Engineering and Computer Sciences, University of California, Berkeley, California 94720, USA*
[e]*Materials Science and Engineering, University of California, Berkeley, California 94720, USA*

Manuscript submitted June 10, 2014; revised manuscript received September 16, 2014. Published October 22, 2014. This was Paper 2290 presented at the San Francisco, California, Meeting of the Society, October 27-November 1, 2013.

Indium (In) plays an important role in the electronics industry, such as in high density bump bonds[1,2] and in low temperature soldering.[3,4] It is also an important component of many electronic and optoelectronic materials, such as indium phosphide (InP), indium selenide, copper indium selenide (CIS), copper indium gallium selenide (CIGS), indium arsenide (InAs), indium gallium phosphide, and indium tin oxide. Many different fabrication techniques exist for these materials, some of the most common being closed space sublimation,[5] metal organic chemical vapor deposition,[6–8] co-evaporation,[9] and molecular beam epitaxy.[10,11] An alternative deposition method is electrochemical deposition[12–21] (ECD), which has the advantages of[13,22] (a) low temperature, ambient pressure deposition, (b) high deposition rate which is easily controllable, (c) low cost equipment and precursors, and (d) high material utilization (as high as 98%). The high material utilization rate is especially important when considering the rarity and expense of indium.[23]

Direct ECD of semiconductors like CIGS,[12–14] CIS,[15] InAs,[16–18] and InP[19–21] have been shown in the literature. InP is particularly interesting due to its ideal 1.34 eV bandgap and similarity to gallium arsenide which recently achieved the highest single junction solar cell efficiency to date (~28%).[24] The highest reported InP efficiency to date is over 20%.[24] While the direct ECD of InP has been claimed in the literature, without reports on the optoelectronic quality,[19] those results could not be reproduced by other groups,[25] nor by our group. This is in part because direct ECD of fully reduced phosphorus from aqueous solution is very difficult without a catalyst, such as nickel,[26,27] as suggested previously by Cattarin et al.[25]

An alternative growth method to direct ECD for InP, as well as for CIS and CIGS, is a two-step method, where precursor In thin films are deposited and then reacted at high temperatures with a phosphorus source. In this growth method, the material utilization of In is largely determined by the process used to deposit it, further motivating the use of ECD. The two-step growth approach has been explored for InP[25,28] and recently a new two-step growth method, named thin film vapor-liquid-solid (TF-VLS), has been developed and demonstrated for InP.[29,30] This TF-VLS growth method is unique due to the fact that thin films can be grown with grain sizes which are orders of magnitude greater than the film thickness on non-epitaxial substrates, breaking with the traditional constraints of vapor phase thin film growth.[5,8] Most importantly, it was demonstrated that In evaporated on Mo foil and phosphorized by the TF-VLS process resulted in InP films of high optoelectronic quality, far surpassing that of previous two-step InP growth methods.

For the two-step growth methods, the starting In thin films must be continuous, planar, and high purity. An optimal InP thin film should be 1–3 μm thick for solar cell applications. Since In approximately doubles in thickness as it is converted to InP, there is an additional constraint of the In film thickness being 2 μm or less. The ECD of In has been explored in the past;[3,4] however, these previous applications do not meet the stringent needs of optoelectronic thin film precursors outlined above. Due to the need for high purity In, organic additives, that are traditionally used to tailor deposition morphology in ECD, may not be used as they may get incorporated into the deposited matrix, creating potential defects, recombination sites, and acting as unintentional dopants in the final InP. Furthermore, we explore In ECD on molybdenum (Mo) foil, a ubiquitously used substrate for high temperature growth due to its chemical stability and high melting point. Electrodeposition of a continuous In film of sub-1 μm thickness on Mo is difficult and has resulted in workarounds such as depositing In on Mo with a copper seed layer[31,32] or depositing In simultaneously with other metals.[12,33,34] This paper reports on the electrodeposition of In thin films directly on Mo foil which meet the aforementioned requirements of thickness, roughness, and purity without the use of organic additives.

Experimental

Indium electrochemical deposition and phosphorization.— A schematic of the electrochemical deposition setup is shown in Fig. 1. A CH Instruments *Electrochemical Workstation* potentiostat was used to carry out the electrochemical deposition. The potentiostat was operated in a 3-electrode cell using an Ag/AgCl reference electrode equilibrated in saturated potassium chloride. Indium metal ingots (99.99% Alfa) flattened into foils were used as the counter electrode. Mo foil, 0.1 mm thick, (99.95% Alfa) was cut into 2×1 cm^2 pieces and Kapton tape was used to mask a 1×1 cm^2 active area to operate as the working electrode. The counter and working electrodes were clamped and suspended parallel to each other in the electrolyte solution by a Teflon block that allowed controllable spacing of the electrodes (held at ~8 mm here). The reference electrode was also placed in the same position relative to the working and counter electrodes by this Teflon block. The deposition bath was continuously stirred using a magnetic

*Electrochemical Society Student Member.
**Electrochemical Society Active Member.
[z]E-mail: maboudia@berkeley.edu; ajavey@eecs.berkeley.edu

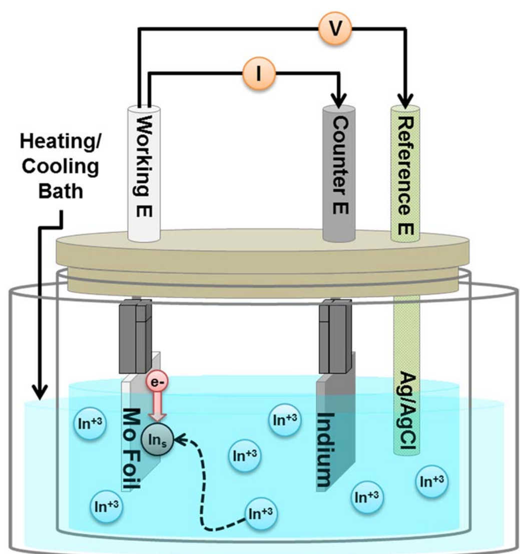

Figure 1. Schematic of electrodeposition bath apparatus with Mo foil as the working electrode, In metal as the counter electrode, and an Ag/AgCl reference electrode. The bath is contained inside a heating/cooling bath for temperature control.

stirrer at 200 RPM during deposition. The electrolyte solution was 1.0 M indium (III) chloride, $InCl_3$ (99.999% Strem). The electrolyte temperature was controlled by an external stirred bath of water (high temperature) or ethanol (low temperature) held at the desired temperature by a hot plate or a cooling unit (FTS FC55).

Cleaning and surface preparation were extremely important to obtain uniform deposits. The Mo foil was degreased by sonication in acetone and then isopropyl alcohol for 30 minutes each. Immediately before deposition, the foil was sonicated in concentrated HCl to remove surface oxide, rinsed with deionized water, and blown dry with nitrogen. The In electrode was prepared by a cleaning dip in aqua regia (HNO_3:HCl 1:3) and then rinsed with DI water and dried with nitrogen. This cleaning process was repeated if the indium surface was not uniformly reflective.

Indium phosphide was grown from the ECD In films by the TF-VLS process reported in detail previously.[29] In short the ECD In was capped with 50–500 nm of E-beam evaporated SiO_2. The stack was then phosphorized in a 1-zone furnace at 750°C and 100 Torr by flowing 10% phosphine in hydrogen (Voltaix 99.9995%). Samples were heated to 750°C under a pure hydrogen gas flow; phosphine gas was introduced once a stable temperature was achieved. Samples were held at the growth temperature for a given duration of 20 – 60 minutes depending on In film thickness and then rapidly cooled with continued phosphine flow.

Chemical, structural and optoelectronic characterization.— The In and InP thin film morphologies were characterized by optical microscopy and scanning electron microscopy, SEM (JEOL 6340F SEM/EDS). Chemical composition was confirmed by X-ray diffraction, XRD (Bruker AXS D8 Discover GADDS XRD) and energy-dispersive X-ray spectroscopy, EDS (JEOL 6340F). Surface chemical composition analysis was performed via X-ray photoelectron spectroscopy, XPS (Kratos Axis Ultra DLD). Depth profiling was achieved by a sequence of sputtering (Kratos Minibeam 1) followed by XPS measurements. Film thickness was determined using a Dektak 150+ surface profiler and surface roughness was characterized using atomic force microscopy, AFM (Digital Instruments Nanoscope III) operated in tapping mode. Current efficiency and average deposit thickness were determined using gravimetric analysis (Denver Instruments Company A-250).

The optoelectronic properties of the InP films were investigated with steady-state photoluminescence (PL) and time-resolved PL (TRPL) apparatuses. The PL apparatus was made up of a helium-neon laser at 632.8 nm with ∼5 μm spot size, and a silicon CCD detector (Andor iDus). The TRPL apparatus used a Mira 900-F Ti-sapphire tunable laser, which produced 200 fs pulses of 800 nm light at 75.3 MHz. The detector was a silicon avalanche photodiode (id Quantique id-100) connected to a TCSPC module (Becker & Hickl SPC-130).

Results and Discussion

Electrodeposition of Indium.— The overall deposition reaction for In on the cathode (Mo foil here) can be summarized as:

$$In^{+3} + 3e^{-} \rightarrow In_{metal} \quad [1]$$

Initial testing found that it was important to use a soluble In metal counter electrode, instead of an insoluble one like platinum. When the anode is In metal, the reverse of Rxn. 1 occurs at its surface, thus avoiding In ion depletion from the deposition bath.

In the experiments reported here, we used constant DC current to drive the deposition so that the total charge passed per unit area, Q (C/cm^2), could be easily controlled by the time duration of the deposition. The main goal was to control the volume of In deposited, assuming the current efficiencies for the various conditions tested to be similar. The theoretical thickness of the In film deposited can be calculated using Faraday's law assuming the In is of uniform thickness and densely packed:

$$h = \eta_j * j * t * \frac{MW_{\mathrm{In}}}{F * n * \rho} = \eta_j * Q * \frac{MW_{\mathrm{In}}}{F * n * \rho} \quad [2]$$

where h is the thickness of the film in cm, η_j is the current efficiency for the process ($0 \le \eta_j \le 1$), j is the current density (A/cm^2), t is the deposition duration (seconds), MW is the molecular weight of In (114.8 g/mol), F is Faraday's constant (96485 C/mole), n is the number of electrons required for the deposition (3 here), and ρ is the density of In, assumed to be the same as bulk In (7.3 g/cm^3). Thus if η_j is assumed to be 1 and Q is chosen to be 1.8 C/cm^2, a 1 μm thick film can be deposited assuming the film is completely continuous. From this analysis we focused primarily on depositing In thin films for Q = 1.8 C/cm^2.

The problem that drives this work is that when one attempts to deposit an indium film with μm thickness on Mo under standard conditions, it is not fully continuous (Fig. 2a). A continuous thin film is considered to be one where indium has no holes exposing the underlying Mo. The nucleation mode observed here can be classically described as the Volmer-Weber growth mode on a foreign substrate,[35] as has been observed previously for In on Mo.[36] Therefore the most important variable to be examined in our films is whether they are continuous when a volume of In corresponding to $h = 1$ μm has been deposited (i.e. at Q = 1.8 C/cm^2). To quantify that, we define the variable fill factor (f) as:

$$f = \frac{Mo\ area\ covered\ by\ In}{unit\ area\ of\ Mo} \quad [3]$$

where a continuous film will have $f = 1$. A simple geometric model helps to motivate the experimental approach. We assume that the average nucleus is representative and spherical in shape. Nuclei are assumed to form with a number density N (measured per unit area). The fill factor is then given by:

$$f = \frac{(projected\ area\ of\ sphere\ covered\ by\ single\ nuclei)(\#\ of\ neclei)}{unit\ area} = \pi r^2 N, \quad [4]$$

with r, the average radius of the sphere, defining the nuclei. If we assume the nuclei grow isotropically, then the spacing of the nuclei will determine the minimum thickness at which a continuous film

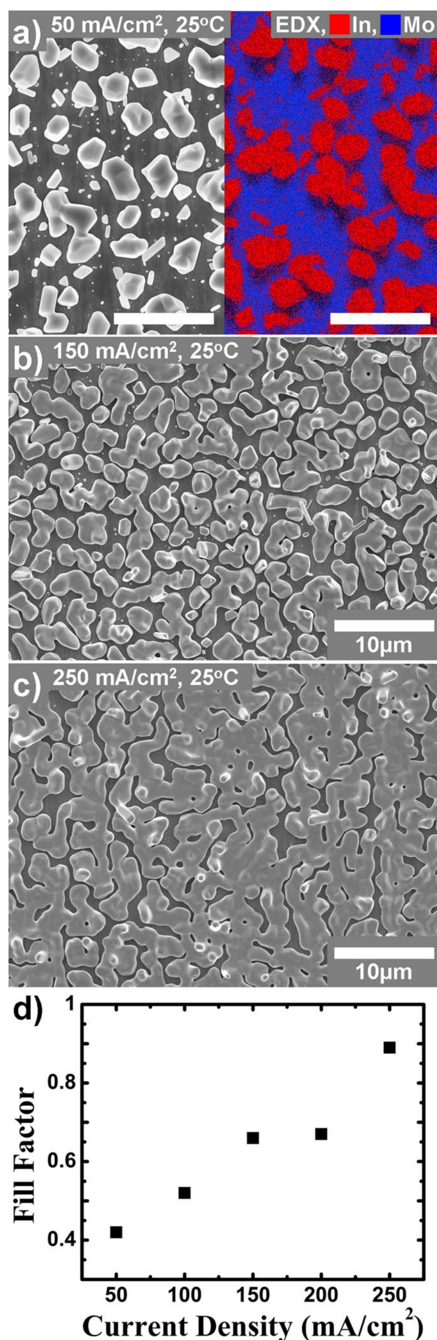

Figure 2. Characteristic SEM images of the In films deposited at room temperature and constant current values of 50 (a), 150 (b), and 250 mA/cm^2(c), with deposition times adjusted to yield Q = 1.8 C/cm^2. Panel (a) also shows an overlay with an EDS elemental mapping indicating which portions of the image are In and which are Mo. The scale bar represents 10 µm. The fill factor was calculated from these SEM images and is plotted versus applied current density (d).

can be achieved. Therefore we must maximize the number density of nuclei, N, in order to minimize the height of a continuous film.

For thin film deposition from vapor phase, it is well known that increasing the flux of the precursor vapor to the substrate's surface increases the number density of nuclei.[35] It is reasonable to expect a similar behavior for ECD. Here the flux of In^{+3} ions is directly controlled by the magnitude of the current density as long as Rxn 1 is the only reaction occurring at the cathode. Accordingly, the effects of varying current density were explored.

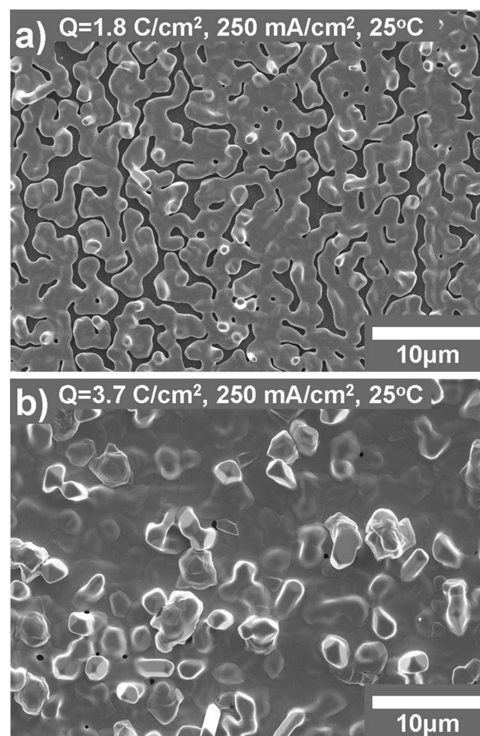

Figure 3. Constant current deposition at room temperature at 250 mA/cm^2 for two total charge conditions: (a) Q = 1.8 C/cm^2, (b) Q = 3.7 C/cm^2. In (b) large indium boulders can be seen dotting the surface.

Effect of current density.— Constant current deposition at room temperature was explored for current densities in the range of 50 to 250 mA/cm^2. As described in the experimental section, the time duration of a given deposition current was chosen such that the same value of Q (1.8 C/cm^2) resulted. Thus, the same volume of In should be deposited at every current density tested, assuming the cathodic efficiency is the same for each condition. This assumption was confirmed by gravimetric analysis of the deposited In showing 90% ± 10% current efficiency for all conditions examined.

The fill factor was calculated from representative SEM/EDS images of the In deposit at each current density. Figure 2a shows a side-by-side image of the In deposit at 50 mA/cm^2 with an EDS elemental mapping depicting In and Mo regions. Characteristic SEM images in Figure 2a–2c show that at higher deposition currents, the fill factor of In on Mo is higher, indicating the nucleation density is higher, as is expected from our analogy to vapor phase deposition. This is consistent with electrochemical theory as well, whereby higher current density requires a higher surface overpotential to drive the reaction, thus reducing the critical nucleus size and allowing higher nucleation density. While the fill factor continued to increase with increasing current density (Fig. 2d), it never reached 100% with a room temperature deposition bath, and 250 mA/cm^2 represents the maximum current the potentiostat could apply while maintaining a reasonable size electrode.

It was found that by doubling *Q*, corresponding to film thickness, h, of 2 µm, a continuous film could be obtained. However, the resulting film was marked with micron tall boulders of In due to the 3-D growth mechanism described previously (Fig. 3b). This type of film thickness non-uniformity is highly undesirable for photovoltaic device fabrication. Attempts to control the size of these boulders using pulse reverse current were made but none of the parameters examined were successful in fully removing the In boulders. The experiments presented here exhausted our capabilities to obtain the desired In thin film by solely controlling the current density and time.

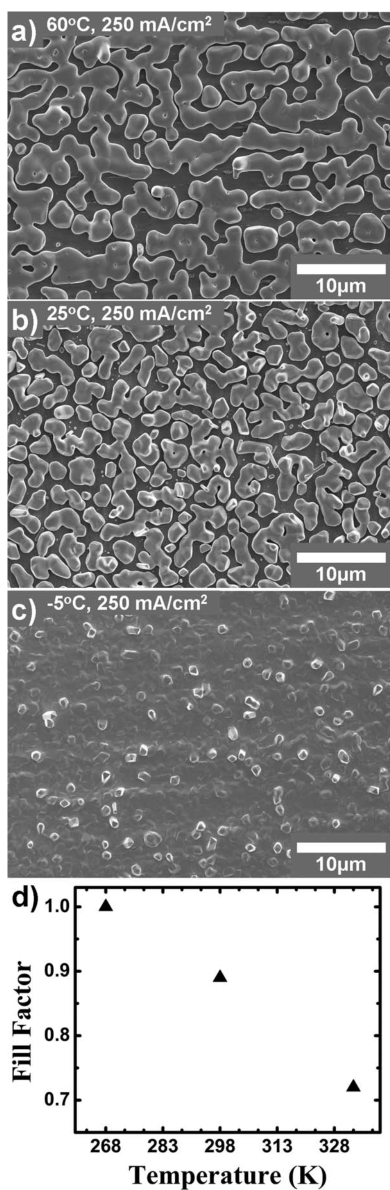

Figure 4. Characteristic SEM images for constant current deposition at 250 mA/cm^2 and Q = 1.8 C/cm^2 for the bath temperatures of 60°C (a), 25°C (b), and −5°C (c). The fill factor was calculated from these SEM images and is plotted versus temperature (d).

Effect of deposition bath temperature.— There are many knobs which can be controlled in electrochemical deposition, one of which is bath temperature. Bath temperature can affected many of the activated processes during deposition including interfacial binding energy and adatom surface diffusion rate. Consequently, we explored the effect of bath temperature, in the range of 60°C to −5°C, on the In film morphology. The total charge used for deposition was set at 1.8 C/cm^2 for all conditions. To achieve maximum fill factor, DC current was applied at 250 mA/cm^2 based on the results discussed in the previous section. Characteristic SEM images of the films deposited at different temperatures are shown in Fig. 4a–4c. The higher bath temperature results in a lower fill factor and a larger grain film, while the lower bath temperature results in a fully continuous film composed of finer In grains. Though temperature affects several governing processes for ECD, we hypothesize the dominating effect is on the adatom diffusion rate, which is known to affect nucleation density in vapor phase deposition.[37,38]

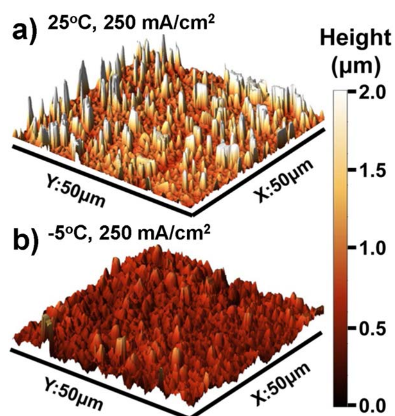

Figure 5. AFM images of the In thin film deposited at 250 mA/cm^2 and Q = 1.8 C at 25°C (a), and −5°C (b). The 3-D growth causing high surface roughness is clearly inhibited at −5°C

Atomic force microscopy was performed on samples deposited at −5°C and 250 mA/cm^2 which showed a root-mean-square roughness of about 100 nm over 50 × 50 µm^2 area. This RMS roughness is ∼3 times lower than the films produced under the same conditions in a room temperature bath (Fig. 5). The In thin films were further characterized by XRD to obtain crystallographic information (Fig. 6a). The films showed preferential orientation for the (101) plane.

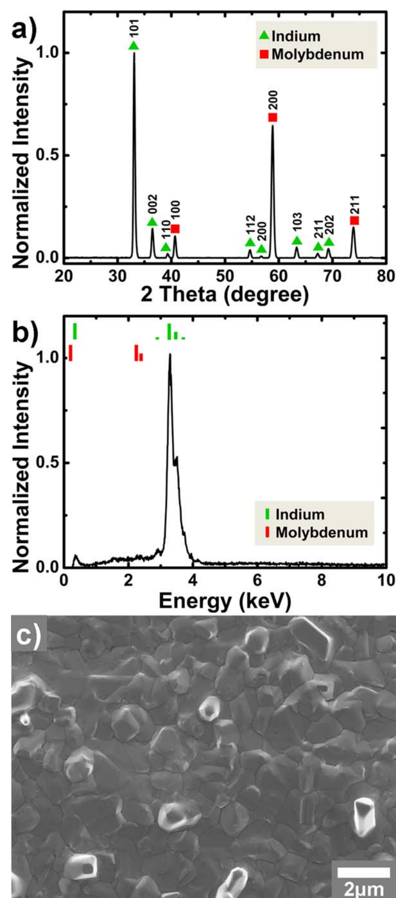

Figure 6. (a) XRD spectrum of the In ECD thin film on Mo deposited at −5°C, normalized to the maximum peak intensity. (b) EDS spectrum of the same In thin film showing no other elemental impurities, normalized to the maximum peak intensity. (c) SEM image of the optimal In thin film displaying a grain size of ∼1 µm.

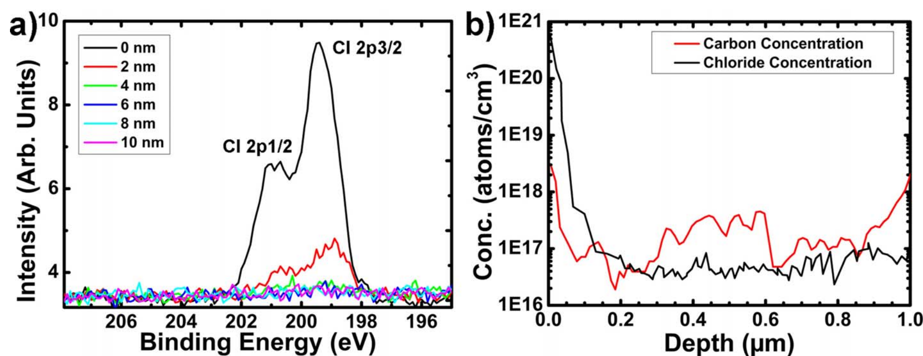

Figure 7. (a) Sputtering XPS was performed on a characteristic sample deposited at -5°C and 250 mA/cm^2 to monitor the chloride contamination. It showed that after a small surface impurity layer, the chloride signal disappeared. (b) Further C^- and Cl^- analysis was done via SIMS which found the chloride impurity in the bulk of the sample to be at most $\sim 5 \times 10^{16}$ /cm^3.

Elemental analysis was performed by EDS (Fig. 6a) which showed that only In was present. Finally, high resolution SEM (Fig. 6c) showed the characteristic surface morphology of the In films. The In thin film produced with these optimal conditions meets all the morphological requirements initially identified.

Further elemental analysis was performed to assess the purity of the deposited In films. Initial XPS analysis showed, in addition to In, the presence of carbon, oxygen, and chlorine but no other elements. As the surface of the film was sputtered away, the signals due to these impurity elements decreased and dropped below the XPS detection limit, (being $\sim$1 atomic percent of the 5nm layer probed) leaving behind only the characteristic In signal. This signifies that the impurity elements are only present in a thin (a few nm) surface layer. The carbon surface contamination is expected from environmental interactions with the sample. The oxygen signal is most likely due to the native oxide which forms on the metal surface. Finally the chlorine contamination (Fig. 7a) has been suggested to be the result of indium chloride crystallites left behind on the surface from the deposition bath. In corroboration of this hypothesis, it was observed that the thickness of the surface chloride layer was dependent on the post deposition rinsing procedure which would affect the amount of salt left behind.

To quantify the bulk purity of the indium, secondary ion mass spectroscopy (SIMS) was performed to track the two major impurities which were observed in XPS, namely, carbon and chlorine. Any bulk chlorine contamination is significant as it is the only elementary species in our bath which cannot be purified out. The SIMS analysis (Fig. 7b) showed that both carbon and chlorine concentrations dropped from high concentrations at the surface to values in the bulk of at most 5×10^{17}/cm^3 for carbon and at most 5×10^{16}/cm^3 for chlorine. The carbon concentration seen here is not considered a major impurity as it is roughly equal to the background concentration of carbon seen in SIMS resulting from residual carbon in the ambient system. It is known that the first several nanometers of analysis in SIMS can have some errors that result in artificially high elemental concentrations.[39] The region can be broadened to the order of magnitude of the surface roughness, $\sim$100nm in the sample examined here. This corresponds well with the depth of the Cl impurity observed in the SIMS results (Fig. 7b). Therefore in this case, the XPS depth profiling data can give a more accurate view of the thickness of the surface contamination which appears to be in the few nm range. This analysis confirms that the In film has a thin surface contamination layer but is otherwise composed of high purity indium.

TF-VLS of ECD in to Obtain InP.— Next we explored the use of ECD In for thin film vapor-liquid-solid growth of InP. Indium films of 1 to 3 μm in thickness were deposited using the optimal deposition parameters described above. Thicker In thin films were obtained by simply increasing Q. The In film was then phosphorized via the TF-VLS technique,[29] for which a process flow schematic has been shown in Fig. 8a. In Fig. 8b, the SEM image shows the surface morphology after phosphorization remains unchanged, which is due to the SiO_x capping layer. The capping layer plays the critical role of confining the In film structurally during the phosphorization process. The cross-sectional SEM (Fig. 8c) shows the Mo substrate beneath a continuous grain of InP greater than 8 μm laterally, despite being only 2 μm tall, a defining characteristic of TF-VLS as described earlier. Figure 8d shows the XRD pattern obtained from the phosphorized ECD In thin film. No In metal peaks can be seen in this spectrum, suggesting that all of the In has been converted to InP. The remaining peaks in the

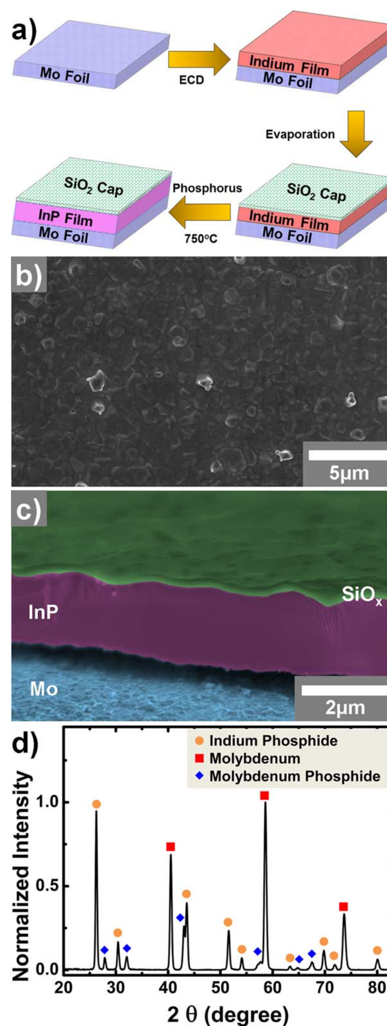

Figure 8. (a) Schematic of the TF-VLS phosphorization of ECD In thin films. (b) Top down SEM of ECD In deposited at optimal conditions after phosphorization. (c) False color cross-sectional SEM of the same sample. The SiO_2 cap can be observed as a thin green line at the top of the sample and the Mo foil can be seen as the rough blue surface beneath the InP thin film (purple). (d) XRD of the phosphorized In thin film showing InP, Mo, and MoP signatures, normalized to the maximum peak intensity.

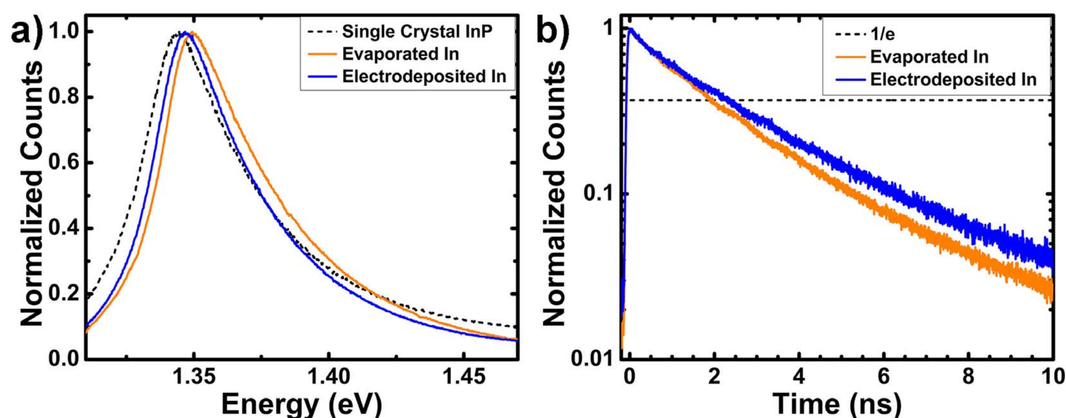

Figure 9. (a) Steady state photoluminescence of an ECD In thin film deposited at optimal conditions after phosphorization at 750°C (blue) compared against an evaporated In thin film phosphorized at the same temperature (orange). Both are compared to a single crystal n-type InP wafer (dashed black) and normalized to the maximum peak intensity. (b) Time resolved photoluminescence of a similar ECD In thin film phosphorized at 750°C (blue) compared to evaporated In phosphorized at the same temperature (orange), normalized to the maximum peak intensity. The dashed line represents the 1/e decay of the maximum peak intensity.

spectrum can be assigned to Mo and MoP. MoP is seen in this spectrum because Mo at the interface with InP reacts with the phosphine gas during the growth process, resulting in a thin MoP layer.

The optoelectronic properties of the InP films were investigated using steady-state photoluminescence (PL) and time resolved photoluminescence (TRPL). For reference, the data were compared to evaporated In of the same thickness, phosphorized at the same temperature, and to single crystal InP(100) (Wafertech) where appropriate (Fig. 9). The PL data show that the ECD In produces InP with similar peak position and full width half maximum (∼1.347 eV and 43 meV, respectively) in comparison to both evaporated indium InP (∼1.349 eV and 46 meV) and single crystal InP wafer (∼1.345 eV and 46 meV). This confirms that optoelectronic-quality InP is grown from the ECD In film. The TRPL data show that the ECD In produces an InP film that performs as well as, if not better than, the InP film obtained from evaporated In with an average 1/e effective carrier lifetime of 2.3 ns. The data further confirms that the In being deposited here is of electronic grade purity.

Conclusions

A simple electrochemical deposition bath was developed to produce continuous, smooth, high purity In thin films of ∼1 μm on Mo foil. Two key developments have been shown here that allowed us to maintain the film morphology as well as its high purity. The first was the ability to control nucleation density of In on Mo with current density and bath temperature. By increasing current density and decreasing bath temperature, a fill factor of 100% could be achieved at ∼1 μm thickness. The second development was the ability to improve the surface roughness of the deposited In by decreasing bath temperature. Using our example system of TF-VLS grown InP, we were able to show that the ECD In films can yield high quality InP thin films, comparable to those obtained from evaporated In films. That no special environment was used to keep the deposition bath pure, outside of those taken in a normal wet laboratory, suggests even higher quality results can be obtained in industrial-level controlled processes. The ability to produce electronic grade In from ECD may be enabling for many In-based technologies, as ECD increases the material utilization rate of In over traditional vacuum deposition techniques. In the example system of TF-VLS InP, a scalable and low cost growth system can be envisioned for wide-scale PV implementation.

Acknowledgments

This work was funded by the Bay Area Photovoltaics Consortium (BAPVC). The modeling of In ECD process and optoelectronic characterization of InP were supported by the Director, Office of Science, Office of Basic Energy Sciences, Materials Sciences and Engineering Division of the U.S. Department of Energy under Contract No. DE-AC02-05CH11231. The XPS measurements were performed at JCAP, Joint Center for Artificial Photosynthesis, a DOE Energy Innovation Hub, supported through the Office of Science of the U.S. Department of Energy under Award Number DE-SC0004993. The SIMS analysis was performed by the Evans Analytical Group.

References

1. D. Hutt and B. Stevens, *2008 58th Electron. Components Technol. Conf.*, 2096–2100 (2008).
2. Y. Tian, C. Liu, D. Hutt, B. Stevens, D. Flynn, and M. P. Y. Desmulliez, *2009 11th Electron. Packag. Technol. Conf.*, 31–35 (2009).
3. F. C. Walsh and D. R. Gabe, *Surf. Technol.*, **8**, 87 (1979).
4. R. Piercy and N. a. Hampson, *J. Appl. Electrochem.*, **5**, 1 (1975).
5. D. Kiriya, M. Zheng, R. Kapadia, J. Zhang, M. Hettick, Z. Yu, K. Takei, H.-H. Hank Wang, P. Lobaccaro, and A. Javey, *J. Appl. Phys.*, **112**, 123102 (2012).
6. C. J. Keavney, V. E. Haven, and S. M. Vernon, *IEEE Conf. Photovolt. Spec.*, 141 (1990).
7. R. H. Moss and J. S. Evans, *J. Cryst. Growth*, **55**, 129 (1981).
8. M. Zheng, Z. Yu, T. Joon Seok, Y.-Z. Chen, R. Kapadia, K. Takei, S. Aloni, J. W. Ager, M. Wu, Y.-L. Chueh, and A. Javey, *J. Appl. Phys.*, **111**, 123112 (2012).
9. R. N. N. Gayen, S. Hussain, D. Ghosh, R. Bhar, and A. K. K. Pal, *J. Alloys Compd.*, **531**, 34 (2012).
10. K. Cheng, *Proc. IEEE*, **85** (1997).
11. A. Cho and J. Arthur, *Prog. Solid State Chem.*, **10**, 157 (1975).
12. C. J. Hibberd, E. Chassaing, W. Liu, D. B. Mitzi, D. Lincot, and a. N. Tiwari, *Prog. Photovoltaics Res. Appl.*, **18**, 434 (2010).
13. R. N. Bhattacharya, *Sol. Energy Mater. Sol. Cells*, **113**, 96 (2013).
14. R. N. Bhattacharya, M.-K. Oh, and Y. Kim, *Sol. Energy Mater. Sol. Cells*, **98**, 198 (2012).
15. R. P. Raffaelle, H. Forsell, T. Potdevin, R. Friedfeld, J. G. Mantovani, S. G. Bailey, S. M. Hubbard, E. M. Gordon, and a. F. Hepp, *Sol. Energy Mater. Sol. Cells*, **57**, 167 (1999).
16. T. Wade, B. Flowers, R. Vaidyanathan, K. Mathe, C. B. Maddox, and J. L. Stickney, *Mater. Res. Soc. Symp. Proc.*, **581**, 145 (2000).
17. T. L. Wade, L. C. Ward, C. B. Maddox, U. Happek, and J. L. Stickney, *Electrochem. Solid-State Lett.*, **2**, 616 (1999).
18. T. L. Wade, R. Vaidyanathan, U. Happek, and J. L. Stickney, *J. Electroanal. Chem.*, **500**, 322 (2001).
19. S. N. Sahu, *J. Mater. Sci. Lett.*, **8**, 533 (1989).
20. S. N. Sahu, *Sol. Energy Mater.*, **20**, 349 (1990).
21. S. Sahu, *J. Mater. Sci. Mater. Electron.*, **3**, 102 (1992).
22. I. M. Dharmadasa and J. Haigh, *J. Electrochem. Soc.*, **153**, G47 (2006).
23. M. Woodhouse, A. Goodrich, R. Margolis, T. L. James, M. Lokanc, and R. Eggert, **3**, 833 (2013).
24. M. A. Green, K. Emery, Y. Hishikawa, W. Warta, and E. D. Dunlop, *Prog. Photovoltaics Res. Appl.*, **21**, 827 (2013).
25. S. Cattarin, M. Musiani, U. Casellato, G. Rassetto, G. Razzini, F. Decker, and B. Scrosati, *J. Electrochem. Soc.*, **142**, 1267 (1995).
26. I. V. Petukhov, *Russ. J. Electrochem.*, **43**, 34 (2007).

27. T. Mimani and S. M. Mayanna, *J. Chem. Sci.*, **109**, 203 (1997).
28. J. Ortega, *An. Quim.*, **87**, 641 (1991).
29. R. Kapadia, Z. Yu, H.-H. H. Wang, M. Zheng, C. Battaglia, M. Hettick, D. Kiriya, K. Takei, P. Lobaccaro, J. W. Beeman, J. W. Ager, R. Maboudian, D. C. Chrzan, and A. Javey, *Sci. Rep.*, **3**, 2275 (2013).
30. R. Kapadia, Z. Yu, M. Hettick, J. Xu, M. Zheng, C.-Y. Chen, A. D. Balan, D. C. Chrzan, and A. Javey, *Chem. Mater.* (2014).
31. Q. Huang, K. Reuter, S. Amhed, L. Deligianni, L. T. Romankiw, S. Jaime, P.-P. Grand, and V. Charrier, *J. Electrochem. Soc.*, **158**, D57 (2011).
32. R. C. Valderrama, M. Miranda-Hernández, P. J. Sebastian, and a. L. Ocampo, *Electrochim. Acta*, **53**, 3714 (2008).
33. R. C. Valderrama, M. Miranda-Hernández, P. J. Sebastian, and a. L. Ocampo, *Electrochim. Acta*, **53**, 3714 (2008).
34. S. M. Lee, S. Ikeda, Y. Otsuka, W. Septina, T. Harada, and M. Matsumura, *Electrochim. Acta*, **79**, 189 (2012).
35. J. A. Venables, G. D. T. Spiller, and M. Hanbucken, *Rep. Prog. Phys*, **47**, 399 (1984).
36. C. M. Pettit, J. E. Garland, N. R. Etukudo, K. A. Assiongbon, S. B. Emery, and D. Roy, *Appl. Surf. Sci.*, **202**, 33 (2002).
37. G. Bales and D. Chrzan, *Phys. Rev. B*, **50** (1994).
38. J. Villain, A. Pimpinelli, L. Tang, and D. Wolf, *J. Phys. I*, **2**, 2107 (1992).
39. J. Ho, R. Yerushalmi, G. Smith, P. Majhi, J. Bennett, J. Halim, V. N. Faifer, and A. Javey, *Nano Lett.*, **9**, 725 (2009).